J Neurophysiol 110: 1426–1440, 2013.
First published July 10, 2013; doi:10.1152/jn.01097.2012.

Excitatory and inhibitory contributions to receptive fields of alpha-like retinal ganglion cells in mouse

Stefano Di Marco,[1,2,4] Dario A. Protti,[2] and Samuel G. Solomon[1,2,3]

[1]*ARC Centre of Excellence in Vision Science, The University of Sydney, Sydney, Australia;* [2]*Discipline of Physiology, School of Medical Sciences and Bosch Institute, The University of Sydney, Sydney, Australia;* [3]*Cognitive, Perceptual and Brain Sciences, University College London, London, United Kingdom; and* [4]*Department of Neuroscience and Brain Technologies (NBT-NTECH), Istituto Italiano di Tecnologia, Genoa, Italy*

Submitted 21 December 2012; accepted in final form 24 June 2013

Di Marco S, Protti DA, Solomon SG. Excitatory and inhibitory contributions to receptive fields of alpha-like retinal ganglion cells in mouse. *J Neurophysiol* 110: 1426–1440, 2013. First published July 10, 2013; doi:10.1152/jn.01097.2012.—The ON and OFF pathways that emerge at the first synapse in the retina are generally thought to be streamed in parallel to higher visual areas, but recent work shows cross talk at the level of retinal ganglion cells. The ON pathway drives inhibitory inputs onto some OFF ganglion cells, such that these neurons show "push-pull" convergence of OFF-excitation and ON-disinhibition. In this study we measure the spatial receptive field of excitatory and inhibitory inputs to OFF-sustained (OFF-S) retinal ganglion cells of mouse, establish how contrast adaptation modulates excitatory and inhibitory synaptic inputs, and show the pharmacology of the inhibitory inputs. We find that the spatial tuning properties of excitatory and inhibitory inputs are sufficient to determine the spatial profile of the spike output and that high spatial acuity may be particularly reliant on disinhibitory circuits. Contrast adaptation reduced excitation to OFF-S ganglion cells, as expected, and also unmasked an asymmetry in inhibitory inputs: disinhibition at light-off was immune to contrast adaptation, but inhibition at light-on was substantially reduced. In pharmacological experiments we confirm that inhibitory inputs are partly mediated by glycine, but our measurements also suggest a substantial role for GABA. Our observations therefore reveal functional diversity in the inhibitory inputs to OFF ganglion cells and suggest that in addition to enhancing operational range these inputs help shape the spatial receptive fields of ganglion cells.

receptive field; contrast adaptation; disinhibition; amacrine cell; bipolar cell

PHOTORECEPTOR SIGNALS are gathered by several types of bipolar cells, each of which carries distinct messages to ganglion cells in the inner retina (Wässle 2004). The major functional division of bipolar cell classes is between those that signal an increase in light intensity (ON bipolar cells) and those that signal a decrease in light intensity (OFF bipolar cells). The functional segregation of ON and OFF signals is important for efficient coding of the retinal image (Balasubramanian and Sterling 2009), but subsequent convergence of ON and OFF pathways is thought to be important for generation of cortical receptive fields (Alonso et al. 2001). Similarly, ON and OFF pathways can converge onto individual bipolar cells (Molnar and Werblin 2007) and retinal ganglion cells (Belgum et al. 1982; Müller et al. 1988), suggesting that their initial segregation is also important for generating the receptive field properties of bipolar and retinal ganglion cells.

The primary model for convergence of ON and OFF pathways are those OFF ganglion cells, in several mammalian retinas, whose morphology is similar to alpha ganglion cells in cat (cat: Boycott and Wässle 1974; mouse: Sun et al. 2002). These ganglion cells receive excitatory input from OFF bipolar cells and in addition a tonic inhibitory input from amacrine cells (van Wyk et al. 2009; Zaghloul et al. 2003). A reduction in light intensity brings about an increase in excitation from bipolar cells and a decrease in tonic inhibition from amacrine cells (disinhibition). In contrast, an increase in light brings about an increase in inhibition. Both increases and decreases in inhibition are thought to reflect modulation of glycinergic input to ganglion cells, particularly that of AII amacrine cells (Manookin et al. 2008; van Wyk et al. 2009). The simplest model of this circuit is that the level of inhibition reflects the signals of ON bipolar cells, as seen through amacrine cells: ON bipolar cell activity increases at light-on and decreases at light-off, and the level of inhibition provided by amacrine cells should track this.

The "push-pull" of excitatory and inhibitory inputs to OFF-sustained (OFF-S) ganglion cells confers an expanded dynamic range (Manookin et al. 2008; van Wyk et al. 2009). Through whole cell recordings from mouse retina we address here two outstanding questions. First, we compare the spatial receptive fields of excitation and inhibition. This is important because the functional advantage of the push-pull arrangement will depend on the relative spatial organization of its elements. We show that the spatial profiles for excitation and disinhibition are similar but that disinhibition is relatively more effective for small stimuli, suggesting that disinhibition contributes to high spatial acuity as well as dynamic range. Second, we establish whether disinhibition at light-off and inhibition at light-on are drawn from the same source. We show that the two forms of inhibition can be dissociated functionally and pharmacologically. This suggests that the two forms of inhibition are derived from different sources, or a single source with highly nonlinear light response.

METHODS

Ethical approval. Measurements described here were made from the retinas of 29 adult mice (*Mus musculus*, C57BL/6J, 4–6 wk, male and female) obtained from the Animal Resource Centre (Perth, Australia). The measurements were made as part of a wider series of

Address for reprint requests and other correspondence: S. Di Marco, Dept. of Neuroscience and Brain Technologies (NBT-NTECH), Istituto Italiano di Tecnologia, Via Morego 30, 16163, Genoa, Italy (e-mail: stefano.dimarco@iit.it).

experiments. Procedures were approved by the institutional (University of Sydney) Animal Ethics Committee and conform to the Society for Neuroscience and National Health and Medical Research Council (Australia) policies on the use of animals in neuroscience research.

Tissue preparation. Animals were dark-adapted for at least 60 min and then euthanized by cervical dislocation. The eyes were enucleated under dim red light, and the rest of the procedures were carried out under infrared illumination. Enucleated eyes were transferred to a petri dish containing carboxygenated Ames medium, and cornea was removed by cutting above the ora serrata. The eyecup was then cut in half, and the remaining tissue was placed in a light-tight box to preserve dark adaptation. From the excised half, the retina was detached from the sclera, placed photoreceptor side down in a recording chamber, and transferred to a microscope stage, where it was continuously perfused with carboxygenated Ames medium heated to 35°C. Cells were viewed on a video monitor coupled to a CCD camera mounted on an Axioskop microscope (Carl Zeiss) illuminated with infrared light.

Electrophysiological recordings and visual stimulation: voltage clamp. Cell-attached and whole cell recordings were obtained from ganglion cells in whole mount retina in voltage-clamp mode with an EPC10 patch-clamp amplifier (HEKA Elektronik). We targeted cells with a soma diameter $\geq$20 μm. Patch electrodes were filled with an intracellular solution containing (in mM) 110 Cs methanesulfonate, 5 tetrabutylammonium, 20 HEPES, 10 EGTA, 1 $CaCl_2$, 4.6 $MgCl_2$, 4 ATP-Na, 0.5 GTP-Na, and 20 creatine phosphate, with 250 U/ml creatine phosphokinase. Voltage-gated sodium currents were blocked by adding 5 mM QX-314 to the intracellular solution. Lucifer yellow (0.2%) was added to the intracellular solutions for cell identification. Ames medium was perfused at 3 ml/min. A liquid junction potential of -15 mV was subtracted from voltage values off-line. Patch pipettes of 5–8 MΩ were used; series resistance usually ranged between 25 and 35 MΩ and was left uncompensated. The chloride reversal potential (E_{Cl^-}) for these solutions was calculated to be approximately -65 mV.

Visual stimuli. Achromatic stimuli were displayed via a calibrated DLP projector (Infocus LP120; refresh rate 60 Hz), imaged through the microscope optics, and focused onto the photoreceptor layer. Visual stimuli were generated by an Apple Macintosh G4 using EXPO (P. Lennie; University of Rochester, Rochester, NY); TTL pulses sent from the stimulus computer to the recording computer were used to synchronize data acquisition. After placement in the recording chamber the retina was continuously exposed to the mean luminance (0.025 cd/m^2). Visual stimuli were uniform circular spots of varying diameter (80, 250, 400, 600, 800, 1,200 μm) and Weber contrast 0.5. The spot could be an increment or decrement of luminance from the background and was presented for 0.5 s. During presentation of a stimulus the remaining portion of the image on the retina was held at the mean luminance. The set of stimuli, which included a blank field of the mean luminance, was presented in a pseudorandom manner.

Contrast adaptation. The adaptor was a large uniform field (diameter 1,200 μm) the luminance of which was modulated in time by a 3-Hz square wave. The adaptor was modulated at the maximum contrast achievable: its Michelson contrast, $(L_{max} - L_{min})/(L_{max} + L_{min})$, was 0.98. After 30 s of exposure to the adaptor, the image was returned to the mean luminance for 0.5 s, and a test stimulus was then presented for 0.5 s. The image then returned to the mean luminance for 0.8 s, after which the adaptor was presented for 3 s. This sequence (test—top-up—test) was repeated until all measurements were carried out. Before adaptation, and 5 min after, we obtained control measurements. In this case the same sequence was presented, but the adapting stimulus was replaced with a uniform field of the mean luminance. Measurements obtained before and after the adaptation protocol were averaged and are referred to in the text as control condition.

Data acquisition. Loose-patch measurement of action potentials was used to establish area-response functions for spike rate. The spike rate was calculated as the mean discharge rate during the 0.5 s of stimulus presentation, averaged over six repeats of each stimulus. Whole cell measurements were used to establish stimulus-evoked currents at each of six holding potentials. Currents were averaged over two presentations of each stimulus. To establish baseline for leak subtraction (described below), the voltage step was initiated 0.7 s before onset of the test visual stimulus and terminated 0.6 s after its offset. Outside this time the cell was held at the resting potential (-75 mV). For contrast adaptation paradigms, the cell was held at the resting potential during exposure to the adapting stimulus.

Conductance analysis. Stimulus-evoked conductance was decomposed into excitatory and inhibitory conductance with a modified version of previously described methods (Borg-Graham 2001; Di Marco et al. 2009; Taylor and Vaney 2002). Stimulus-evoked synaptic currents were elicited at holding potentials ranging from -100 to $+25$ mV every 25 mV. Currents contained residual potassium current with a time-dependent inactivation component in response to depolarizing potentials above -25 mV, which was removed by extracting the currents 0.2 s before and 0.2 s after the visual stimulus, finding the slope of the line that joined these measurements, and subtracting this from the stimulus-evoked currents. The mean current over the 0.15–0.2 s following offset of the visual stimulus was then added back to the detrended currents. Mean amplitude of stimulus-evoked synaptic currents was calculated in nonoverlapping bins of 0.01 s as the difference between the measured current and the average baseline current over the 0.2 s before stimulus presentation. These were used to construct current-voltage (*I-V*) curves at 0.01-s resolution. From these the reversal potential (E_{rev}) and total conductance (G_T) were estimated as the voltage at which current was 0 pA and the slope of a linear fit to the *I-V* curve, respectively. Excitatory and inhibitory conductance (G_e and G_i) were estimated as follows:

$$G_e(t) = \frac{G_T(t) \times [E_{rev}(t) - E_{inh}]}{E_{exc} - E_{inh}} \quad (1)$$

$$G_i(t) = \frac{G_T(t) \times [E_{rev}(t) - E_{exc}]}{E_{inh} - E_{exc}} \quad (2)$$

where E_{exc}, the reversal potential of excitatory currents, was considered to be 0 mV and E_{inh}, the reversal potential of chloride, was estimated to be -65 mV.

Tonic conductance analysis. The impact of contrast adaptation or drug application on tonic synaptic inputs was estimated as changes in tonic excitatory and inhibitory conductance. These measurements were made in cells where no changes in leak currents or access resistance occurred during recordings, and it was assumed that the drugs used affected only neurotransmitter receptors and not voltage-gated currents in the cells under recording. This assumption is in principle correct, as SR95531 and strychnine only target $GABA_A$ and glycine receptors, respectively. Currents required to hold the cell were measured in control conditions and in the presence of a drug or during contrast adaptation. In each case the currents were measured over 0.5 s during presentation of a blank screen of the mean luminance; holding potentials were the same as above. The average difference in current (for contrast adaptation: adapted-control; for drug application: drug-control) was used to construct *I-V* curves. These were then used to calculate change in G_T and E_{rev}, from which G_e and G_i were obtained as above (*Eqs. 1* and *2*).

Difference-of-Gaussians model of spatial receptive field. Spatial tuning of spike rate and synaptic conductances was characterized by finding the best predictions of a difference-of-Gaussians (DoG) model of the receptive field (Enroth-Cugell and Robson 1966; Rodieck 1965; Rodieck and Stone 1965). The DoG model assumes that the receptive field consists of a narrow, center Gaussian concentric with a broader surround Gaussian of opposite polarity:

$$R(s) = \kappa_c \cdot erf(s/d_c)^2 - \kappa_s \cdot erf(s/d_s)^2 \quad (3)$$

where s is the diameter of the stimulus, *erf* is the error function, κ_c and d_c are the strength and diameter of the center, and κ_s and d_s are the strength and diameter of the surround. For disinhibition the relevant response metric is the magnitude of the reduction in conductance (that is, negative values of conductance), so in this case the model predictions were multiplied by −1. In each case we found the best predictions of the DoG model with the function *lsqcurvefit* in the MATLAB environment, which finds the parameters of the model that minimize the mean square error between the observations and the model predictions. In finding the best predictions of the DoG model, we constrained the size of the surround to be always larger than the size of the center.

To provide a clear index of the degree of size selectivity we calculated from the model a suppression index (SI), such that $SI = 1 - (R_{large}/R_{peak})$, where R_{large} is the response generated by the largest spot size and R_{peak} is the peak response. An SI of 1 indicates that the ganglion cell did not respond to large uniform fields, and an index of 0 indicates that there was no spatial tuning.

Morphological reconstructions. Digital photomicrographs of the recorded cell were taken immediately after the end of the recording session. At the end of the experiments retinas were fixed in paraformaldehyde (4% in PBS) for 30 min and then washed in 0.2 M PBS three times for 10 min each. Fixed retinas were incubated with an antibody to Lucifer yellow (rabbit IgG, 1:10,000; Invitrogen) overnight at room temperature and then incubated with Alexa 594 conjugated to goat anti-rabbit IgG (1:500; Invitrogen) for 16 h. Images were acquired with a confocal microscope (Zeiss LSM 510 Meta or Leica SPE-II).

RESULTS

In the following we characterize spatial summation in a class of OFF-S ganglion cells of the mouse retina. Measurements from a total of 26 neurons are included, drawn from a larger sample of ganglion cells encountered during the course of these experiments. We targeted ganglion cells with large soma (>20 μm in diameter). With loose-patch recordings we recorded action potentials and identified those neurons that showed sustained responses to light decrements. We then generated a gigaohm seal and proceeded to whole cell recordings. All neurons identified as OFF-S on the basis of action potential measurements showed the same temporal profile of excitatory and inhibitory synaptic conductance, as described below. In some cells, we were unable to maintain loose-patch conditions (~100 MΩ) and a gigaohm seal was reached before quantitative measurement of spike response could be made. In these cases we passed to whole cell configuration and used the characteristic patterns of excitatory and inhibitory synaptic conductances to confirm functional classification.

In 15 of 26 cells in which we made conductance measurements we were able to recover morphology after the experiment; in a further 11 cells we photographed the cell in the chamber but were unable to recover the cell after histology. Soma size was 20–24 μm, and radial dendrites extended over 235 μm (SD 69, $n = 15$). A robust morphological taxonomy of ganglion cells in the mouse retina is not yet available. From their soma size and dendritic arborization all the cells that we recovered had morphologies consistent with class A2 (outer) or class C2 (outer) of Sun et al. (2002). Previous work suggests that OFF-S cells are C2 (outer) (van Wyk et al. 2009). OFF-S cells in mouse are possible homologs of the OFF alpha cell in cat retina (Boycott and Wässle 1974). OFF-S cells in mouse are likely to be homologs of the OFF delta ganglion cell in guinea pig retina, which show sustained visual response; OFF alpha cells in guinea pig show transient response (Manookin et al. 2008). For the remainder of this paper we refer to these cells as OFF-S cells.

Synaptic inputs to OFF-S ganglion cells in mouse retina. Figure 1 shows the characteristic response of cells included in our analyses. When light was withdrawn from the receptive field (light-off), all cells responded with a sustained increase in spike rate; when light was added to the field, spike rate decreased below the maintained rate and then increased sharply on return to the mean luminance. The synaptic inputs generating these responses are also shown in Fig. 1. To establish excitatory and inhibitory conductance we held the ganglion cell at each of several potentials while we added or withdrew light to the receptive field. From the set of measurements we could measure, at a resolution of 10 ms, the changes in conductance brought about by each stimulus. By tracking the magnitude and direction of these changes in conductance we could extract the contribution of excitatory and inhibitory inputs to the neuron (see METHODS). Recall that OFF-S cells receive excitatory synaptic input from OFF bipolar cells and tonic inhibitory input from amacrine cells. Figure 1 shows that increased spike rate at light-off reflects increased excitatory input from OFF bipolar cells (Fig. 1, *A–C*, dashed lines) and the removal of tonic inhibition from amacrine cells (Fig. 1, *A–C*, solid lines). Reduction in spike rate at light-on reflects a small reduction of tonic excitatory input from OFF bipolar cells and a large increase in inhibitory input from amacrine cells (Fig. 1, *D–F*).

Figure 1*G* shows average spike response, and Fig. 1*H* shows average synaptic conductances, across the population of neurons included in the following analyses. Consistent with the classification of these neurons as OFF-S ganglion cells, spiking activity increases at light-off and is sustained for the duration of stimulus presentation (0.5 s). Increase in excitatory conductance and removal of tonic inhibition show a similar sustained time course. The time courses of spike response and synaptic conductance are consistent with previous descriptions of OFF-S alpha-like cells in mouse retina (van Wyk et al. 2009) and OFF-delta cells in guinea pig retina (Manookin et al. 2008). The time courses of spike response and synaptic conductance are slightly different: spike response shows an initial burst of action potentials, but conductance is maintained at the same level throughout the stimulus. We have not explored this further, but it may reflect changes in threshold due to depolarization-induced inactivation of sodium channels (van Wyk et al. 2006; Platkiewicz and Brette 2011).

Center-surround interactions in receptive fields of OFF-S ganglion cells. The morphology, spike response, and pattern of synaptic conductance were similar for all cells included here, but area summation tests revealed two different functional response types. For each cell we measured area-response curves by confining the light decrement to a circular patch, the diameter of which was varied. Figure 1 illustrates these measurements for the example cell. Whether the response metric is spike rate, excitation, disinhibition, or inhibition, response at first increased with stimulus diameter. In some cells response then plateaued and did not change as stimulus diameter increased; in others response peaked and then declined sharply for larger sizes (Fig. 2). To characterize this we calculated the suppression index (SI), which is simply the reduction in re-

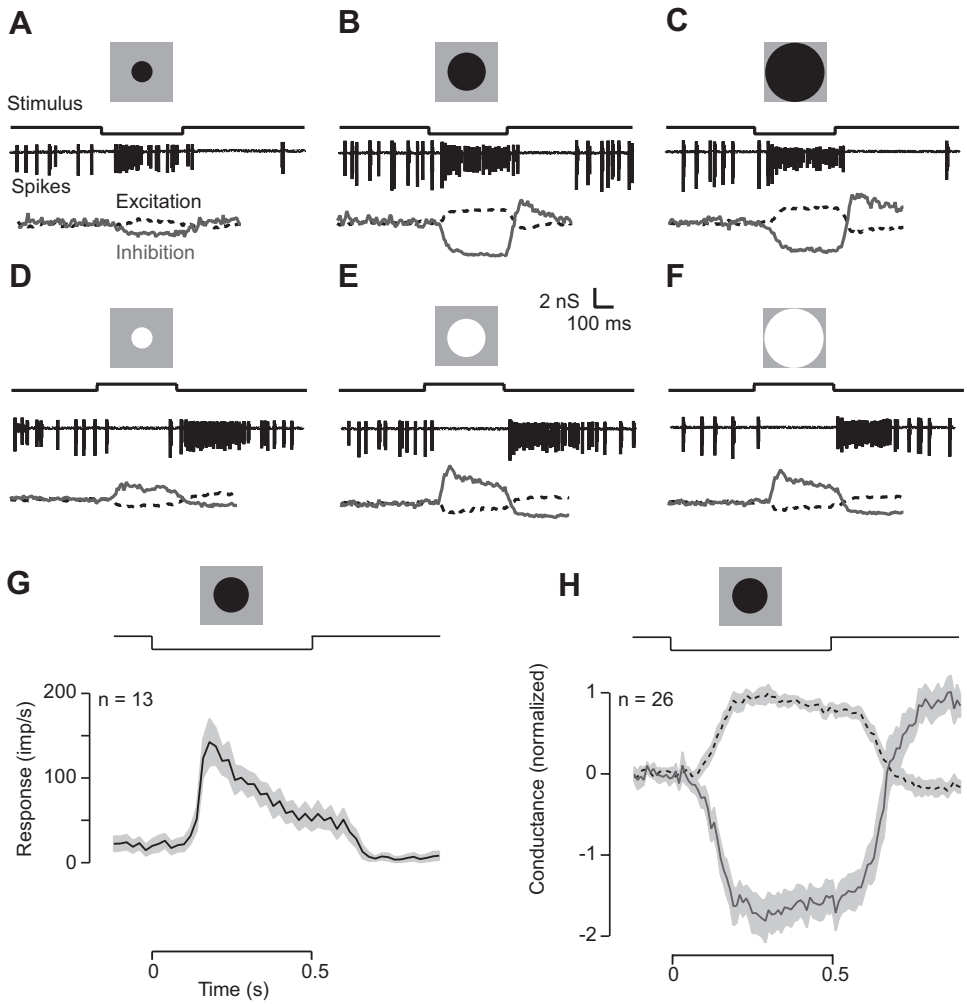

Fig. 1. Spike response and synaptic inputs to OFF-sustained (OFF-S) ganglion cells in mouse. *A–F*: response of a representative OFF-S ganglion cell. *A–C*: response to light decrements (light-off). *D–F*: response to light increments (light-on). The stimulus was confined to spots of diameter 80 μm (*A*, *D*), 250 μm (*B*, *E*), or 1,200 μm (*C*, *F*). *Top*: temporal profile of the stimulus (duration 0.5 s). *Middle*: action potentials recorded in on-cell configuration. Spike rate increases at light-off and is reduced at light-on. *Bottom*: excitatory conductance (dashed lines) and inhibitory conductance (solid lines) subsequently recorded in whole cell configuration. Light-off brings about an increase in excitation and a withdrawal of inhibition. Light-on brings about a small reduction in excitation and a large increase in inhibition. *G*: average spike rate over 13 OFF-S cells in response to a decrement of light confined in a spot of 400 μm. Spike response is sustained over the duration of the stimulus. *H*: average excitatory (dashed line) and inhibitory conductance (solid line) for 26 OFF-S cells for the same stimulus as in *G*. Excitatory conductance is sustained over the duration of the stimulus. Inhibitory conductance is suppressed (disinhibition) for the duration of the stimulus. Throughout this report, stimulus-evoked decrease in inhibitory conductance is referred to as disinhibition and stimulus-evoked increase in inhibitory conductance is referred to as inhibition. Gray regions in *G* and *H* show $\pm$1 SE.

sponse as the stimulus is made larger than optimal—a value of 0 implies no reduction in response, and a value of 1 implies that response was completely attenuated by making the stimulus large.

Figure 2*F* shows SI obtained for excitatory conductance (*x*-axis). There are two clusters of cells. One group ("tuned," 10/26) has SI $>$ 0.4. A second group ("untuned," 16/26) has SI $<$ 0.4. In the following we will always define cells as "tuned" or 'untuned' from the SI measured for excitation. Across tuned cells SI for excitatory conductance was 0.67 (SD 0.09, $n = 10$) and for untuned cells was 0.12 (SD 0.03, $n = 16$). Figure 2, *A* and *B*, show the morphology of one tuned and one untuned cell; there are no obvious differences.

Area-response curves for excitation and inhibition were similar in shape: when excitatory conductance was tuned, so were disinhibition at light-off and increases in inhibition at light-on. Filled circles in Fig. 2*F* compare SI for excitation and disinhibition (both measurements obtained for light-off). The average SI for disinhibition was 0.58 (SD 0.04, $n = 10$) for tuned cells and 0.10 (SD 0.08, $n = 16$) for untuned cells. Figure 2*F* also compares SI for excitation at light-off with that obtained for inhibition at light-on: SI of inhibition was 0.65 (SD 0.12, $n = 10$) for tuned cells and 0.19 (SD 0.09, $n = 16$) for untuned cells. Paired *t*-test of SI for excitation and inhibition at light-off revealed no statistical difference in tuned ($P = 0.31$) or untuned ($P = 0.30$) cells. Similar comparisons of SI for inhibition at light-on and disinhibition at light-off, or for excitation at light-off and inhibition at light-on, also revealed no significant differences (*P* values from 0.28 to 0.63).

For 11 cells we were able to obtain area-response curves for action potentials before gaining whole cell access (Fig. 1). This allowed us to compare area response for spike output with that of the synaptic inputs (Fig. 2*F*). Four cells with tuned excitatory (and inhibitory) conductance also showed sharp tuning in area response for spike rate (mean SI 0.75, SD 0.21). Seven cells showing untuned conductance also showed little tuning in area response in extracellular recordings (mean SI 0.05, SD 0.05). In summary, when area-response curves for excitation were strongly tuned, so were area-response curves for inhibition, and so were those for spike rate.

In the mesopic light levels used here, both rod and cone photoreceptors, and their postsynaptic circuits, should be responsive to light stimulation. In the case of ganglion cells recorded from the ventral retina, however, it is possible that only rod inputs will contribute to light signaling, as our light source does not substantially activate the short-wavelength-sensitive (ultraviolet) cones, which are numerically and physiologically dominant in mouse ventral retina (Szél et al. 1992; Wang et al. 2011). Given that spatial tuning is less prominent in rod pathways (Derrington and Lennie 1982), lack of modulation of ultraviolet cones will reduce the likelihood of observing strong receptive field surrounds in ganglion cells of the

ventral retina. For the neurons included in the above analyses, we did not record the location of the ganglion cell in the retina.

To see whether the variability in strength of the receptive field surround was due to location of the ganglion cell in the retina, in separate experiments we made targeted recordings to dorsal or ventral retina, isolated under the dissection microscope by landmarks in the choroid (Wei et al. 2010). In recordings from the retina of three mice we obtained area-response curves for spike response from eight OFF-S cells in the dorsal retina and five OFF-S cells in the ventral retina. All of these cells showed weak surrounds, with SI $<$ 0.4. In two OFF-S cells in dorsal retina, we increased the background luminance from 0.025 cd/m^2 to 2.5 cd/m^2 to test whether higher luminance levels may unmask stronger surrounds. The area-response curves were no different at higher luminance. In the same experiments we recorded from five ON-sustained alpha-like (ON-S) ganglion cells in dorsal retina and 6 ON-S ganglion cells in ventral retina. Three ventral ganglion cells, and three in the dorsal retina, showed clear evidence of a receptive field surround: response was suppressed by making the stimulus large. Spatially tuned ON cells were encountered immediately before and after untuned OFF-S cells. We conclude that untuned cells can be found in both dorsal and ventral retina and that the absence of receptive field surround was not due to pathology or luminance level. We cannot exclude the possibility that tuned OFF-S ganglion cells are found only in dorsal retina.

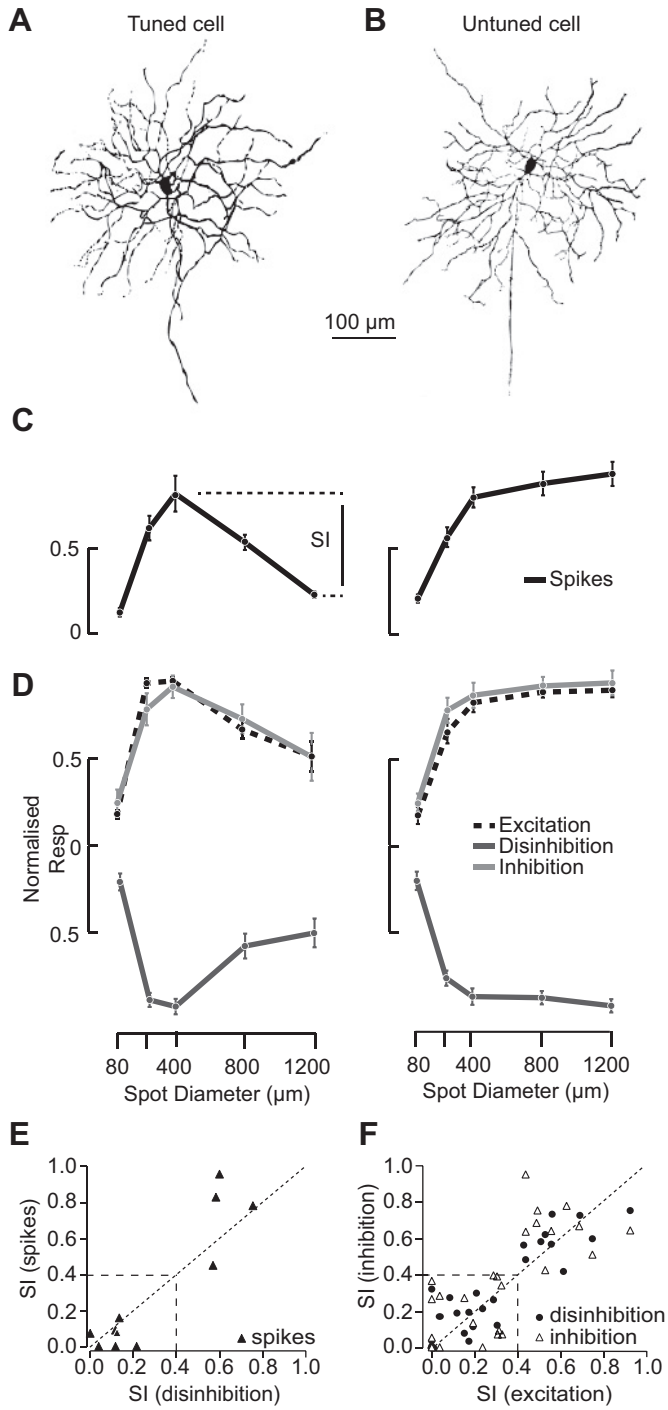

Spatial summation in OFF-S ganglion cells. Figure 2 also shows the average area-response functions of tuned and untuned cells for spike rate and three types of synaptic conductance. In each case area-response functions were normalized to the maximum observed response before averaging. Figure 2*C* shows area response for spike response; Fig. 2*D* shows the magnitude of excitatory conductance and disinhibitory conductance at light-off, along with the increase in inhibitory conductance at light-on. To characterize spatial summation in each case we fit a DoG model (Enroth-Cugell and Robson 1966; Rodieck 1965; Rodieck and Stone 1965) to area-response tuning curves of individual cells (fits not shown). From these fits we extracted the size of putative center and surround mechanisms of the receptive field.

Figure 3 compares the size of the center or surround mechanisms for excitation and the two forms of inhibition, for both tuned and untuned cells. The reader should note that in untuned cells the parameters that describe the surround mechanism of a receptive field are poorly constrained but those that describe the center mechanism are better constrained.

Figure 3*A* compares the size of the center and surround mechanisms of excitatory synaptic input (G_e). Center size is on average 260.3 μm (SD 58.3, $n = 26$). Among tuned cells the size of the surround is highly variable and is not correlated to center size. Figure 3*B* shows counterpart plots for disinhibition at light-off; the size of the center mechanism is less than that for excitation, on average 189.8 μm (SD 38.7, $n = 26$), and the size of the surround is again highly variable. Similar distributions were seen for inhibition at light-on (not shown).

Fig. 2. Receptive field organization in OFF-S retinal ganglion cells. *A*: confocal images of an OFF-S cell with center-surround receptive field organization ("tuned"). *B*: confocal images of an OFF-S cell without center-surround organization ("untuned"). *C*: average area-response function for spike rate. *Left*: tuned cells ($n = 4$). *Right*: untuned cells ($n = 7$). Responses obtained for light-off. To characterize the tuning curves we calculated a suppression index (SI; see METHODS). An SI of 1 indicates no response to a large field; values of 0 indicate response to a large field was at least as vigorous as that to smaller fields. *D*: area-response functions for synaptic conductances: averages for 10 tuned cells and 16 untuned cells. Responses for excitation and disinhibition were obtained for light-off. Responses for inhibition were obtained for light-on. Error bars in *C* and *D* show $\pm$1 SE. *E*: comparison of SI for spike rate and for disinhibition, both obtained for light-off. An SI of 0.4 segregates tuned (SI $>$ 0.4) and untuned (SI $<$ 0.4) cells. *F*: comparison of SI for excitation and SI for 2 types of inhibitory conductance: disinhibition and inhibition. SI for excitation and disinhibition was obtained from response to light-off; SI for inhibition was obtained from response to light-on. Cells with tuned excitation show tuned disinhibition and tuned inhibition.

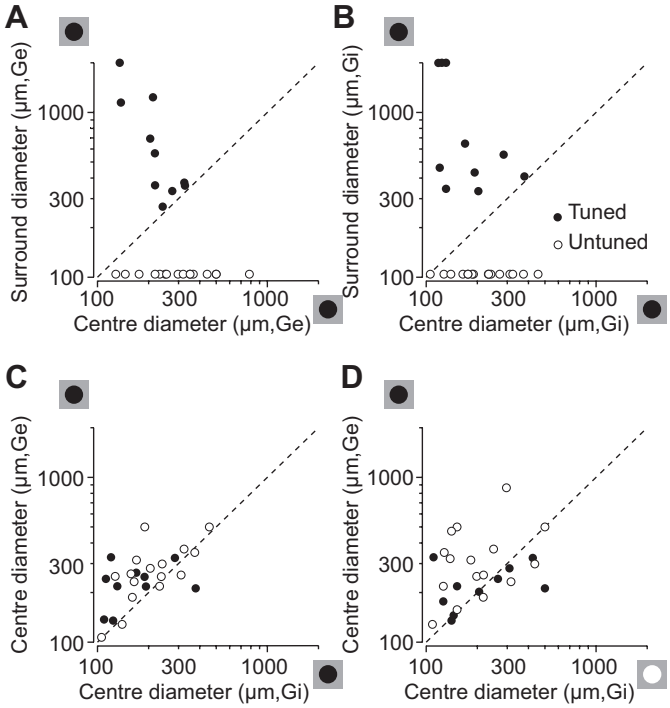

Fig. 3. Receptive field size of synaptic inputs onto OFF-S retinal ganglion cells. *A*: comparison of center and surround diameter for excitation (G_e): responses obtained for light-off. Both tuned cells and untuned cells are shown. Measurements of surround size in untuned cells are poorly constrained; these cells are plotted parallel to the *x*-axis to indicate the range of center sizes encountered. *B*: comparison of center and surround diameter for disinhibition (G_i). Conventions as in *A*. *C*: comparison of center size for excitation and disinhibition. Most points plot above the unity line, so the space constant of excitation is larger than that of disinhibition. Conventions as in *A*. *D*: comparison of center size for inhibition (obtained with light-on) and excitation (obtained with light-off). Excitation space constant is larger than that of inhibition. Conventions as in *A*. Values > 2,000 plot at the axis limits.

Figure 3*C* compares center size for excitation and disinhibition at light-off. The two measurements are correlated ($r = 0.49$, $p = 0.03$; Pearson's correlation on log-transformed data), and the majority of data points lie above the unity line, showing that the summation area of disinhibition was usually less than that of excitation. This difference was seen when we considered tuned and untuned cells separately. For tuned cells receptive field center size for excitation was 228.4 μm (SD 32.3) and for disinhibition was 168.9 μm (SD 36.5; $n = 10$; $P = 0.001$ vs. excitation, paired *t*-test). In untuned cells the center size of excitation was 292.3 μm (SD 46.7) and for disinhibition was 210.7 (SD 43.3; $n = 16$, $P < 0.001$). Figure 3*D* compares center size for excitation at light-off and inhibition at light-on: in this case there is no obvious correlation ($r = 0.24$, $P = 0.23$) and no obvious bias; the ratio of inhibitory to excitatory center size was on average 0.88 (SD 0.46, $n = 26$; $P = 0.19$). Center size of inhibition at light-on and disinhibition at light-off were correlated ($r = 0.62$, $p = 0.001$) and unbiased (0.94, SD 0.34) (not shown). We compared surround sizes in a similar way but saw no clear relationships (not shown), but this may simply reflect the high variability in estimated surround sizes.

Figure 3*C* suggests that disinhibition draws input from a slightly smaller region of the retina than does excitation. Amacrine cells usually gather input from several or many bipolar cells. Spatial summation in amacrine cell inputs is likely to reflect this, and we therefore expected that, if anything, disinhibition would draw input from a larger area of the retina than excitation. Figure 3 and the analyses above suggest that this is not the case. Figure 4 directly compares conductance measured with small and large stimuli. For the smallest size tested (80 μm), responses were dominated by disinhibition: disinhibition was 1.79 times greater than excitation (SD 0.37, $n = 26$; significantly greater than 1: $P < 0.001$). For larger sizes this ratio ranged from 0.98 to 1.10. Similar obser-

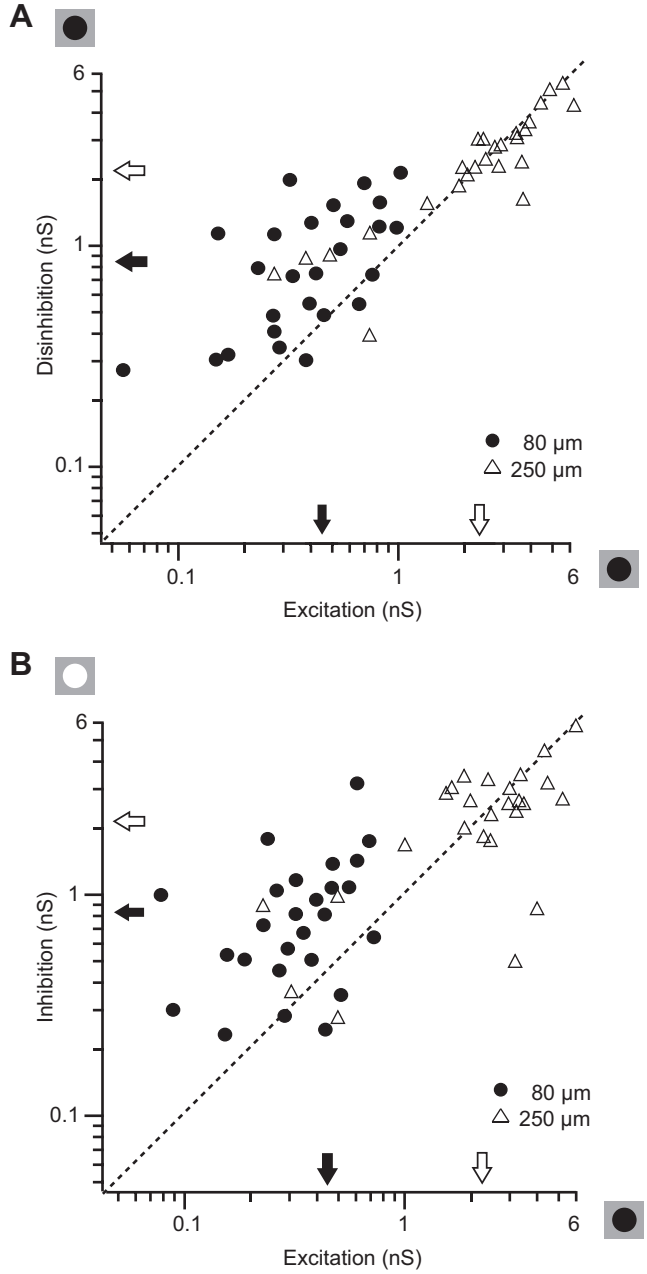

Fig. 4. Small stimuli evoke strong inhibitory conductance. *A*: comparison of magnitude of excitation and disinhibition for the smallest stimulus (80 μm) and the next largest stimulus (250 μm): responses obtained for light-off. For the smallest stimulus, most points plot above the unity line, showing that the magnitude of disinhibition is greater than that of excitation. This is not the case for the larger stimulus, which also evokes larger conductance. *B*: comparison of magnitude of excitation (obtained with light-off) with inhibition (obtained with light-on). Conventions as in *A*. Inhibition is relatively stronger for the smallest stimulus.

vations can be made for inhibitory input at light-on (Fig. 4*B*). Inhibitory input at light-on in response to the smallest stimulus was 1.67 (SD 0.48, $n = 26$; $P < 0.001$) times greater than excitatory input at light-off; for larger sizes this ranged from 0.93 to 1.08. We conclude that the mechanisms that provide excitation draw signals from a slightly larger area of the retina than those that provide disinhibition, or increases in inhibition.

Synaptic modulation during contrast adaptation. It is generally thought that a single source of tonic inhibition is removed during light-off (disinhibition) and increased during light-on (van Wyk et al. 2009; Zaghloul et al. 2003). In the following we provide evidence that this is not the case, because the two forms of inhibition have very different sensitivity to contrast adaptation. During prolonged exposure to high-contrast modulation of a large disk (diameter 1,200 μm) we measured responses to a test probe every 5 s. This allowed us to construct area-response curves for the adapted state that could be compared to those obtained before adaptation and after 5 min of recovery, in which the "adaptor" was a blank screen of the mean luminance. In the following we pool data from all cells tested, because the effects of adaptation on spike response and synaptic inputs were not distinguishable in tuned and untuned cells.

Previous work has shown that contrast adaptation in ganglion cells arises in two general mechanisms—a reduction in the magnitude of excitatory synaptic inputs and additional effects on voltage-gated conductance involved in spike generation (Kim and Rieke 2001, 2003; Weick and Demb 2011). In the following recordings we isolated the synaptic mechanisms by blocking voltage-gated sodium and potassium channels. We first confirm that contrast adaptation reduces spike response and the magnitude of excitatory synaptic inputs and show its effect on the spatial profile of the receptive field; we then characterize the impact of adaptation on inhibitory inputs, which has not been explored.

Figure 5 shows synaptic conductance during presentation of the probe stimulus in a representative OFF-S cell, obtained in control conditions and during contrast adaptation. Response in the control condition is the average of measurements made before and after the adaptation protocol. The reader should note that these analyses focus on the stimulus-evoked response; changes in the tonic level of conductance are invisible to this analysis and are discussed below. Figure 5, *A* and *B*, show synaptic conductance in response to light-off for two probe diameters: a small size (400 μm; Fig. 5*A*) and the largest size tested (1,200 μm; Fig. 5*B*). In both cases contrast adaptation reduced excitatory conductance at light-off but produced no change in the disinhibitory conductance. Figure 5, *C* and *D*, show similar traces, but for light-on. Contrast adaptation reduced stimulus-evoked inhibition. Contrast adaptation therefore unmasks a striking difference in the functional properties of inhibition and disinhibition, challenging the idea of a common origin of this mechanism.

For most cells light-on was associated with a small reduction in excitatory conductance (Fig. 5, *C* and *D*). This "disexcitation" was generally reduced by contrast adaptation. For the cell in Fig. 5, excitatory conductance during presentation of a 400-μm spot was -0.41 nS in control conditions and -0.33 nS during adaptation; for a 1,200-μm spot these were -0.79 and -0.29 nS, respectively. Across the population of cells excitatory conductance for a 400-μm spot was -0.35 nS in control conditions and -0.18 nS during adaptation (SD 0.41 and 0.12, respectively; $n = 14$, $P = 0.12$, paired t-test); for a 1,200-μm spot these were -0.40 and -0.13 nS, respectively (SD 0.48 and 0.23; $n = 14$, $p = 0.024$). In one ganglion cell adaptation reversed the polarity of excitatory conductance for light-on at all spot sizes; we did not include the cell in these analyses.

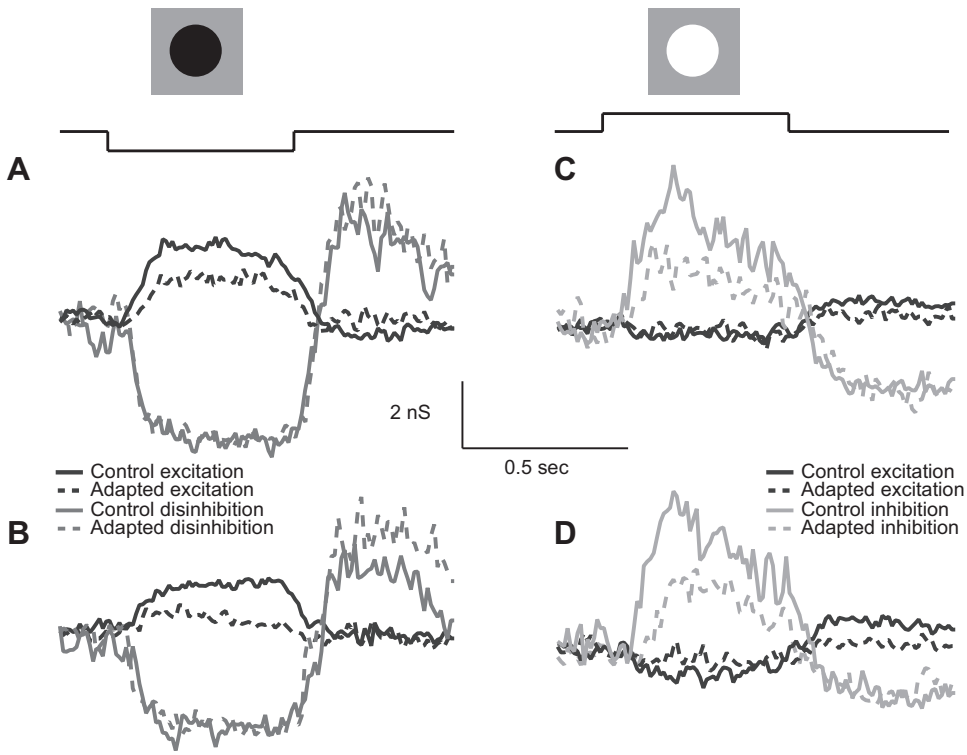

Fig. 5. Impact of contrast adaptation on a representative OFF-S retinal ganglion cell. *A* and *B*: response to light decrements (light-off). *C* and *D*: response to light increments (light-on). The stimulus was confined to spots of diameter 400 μm (*A* and *C*) or 1,200 μm (*B* and *D*). *A* and *B*: stimulus-evoked excitation is reduced during contrast adaptation (black dashed lines) compared with control conditions (black solid lines). Disinhibitory inputs do not change during contrast adaptation (gray dashed lines) compared with control condition (gray solid lines). *C* and *D*: inhibitory inputs are reduced during contrast adaptation (gray dashed lines) compared with control condition (gray solid lines).

Application of repeated-measures ANOVA showed significant effect of adaptation on excitatory conductance across the sample of cells [$F(1,52) = 4.94$; $P = 0.045$] but no effect of size [$F(4,52) = 1.96$; $P = 0.12$]. These are small responses and therefore difficult to characterize reliably, so we have not explored them further. Nevertheless, this analysis suggests that, unlike for disinhibition, contrast adaptation reduces disexcitation.

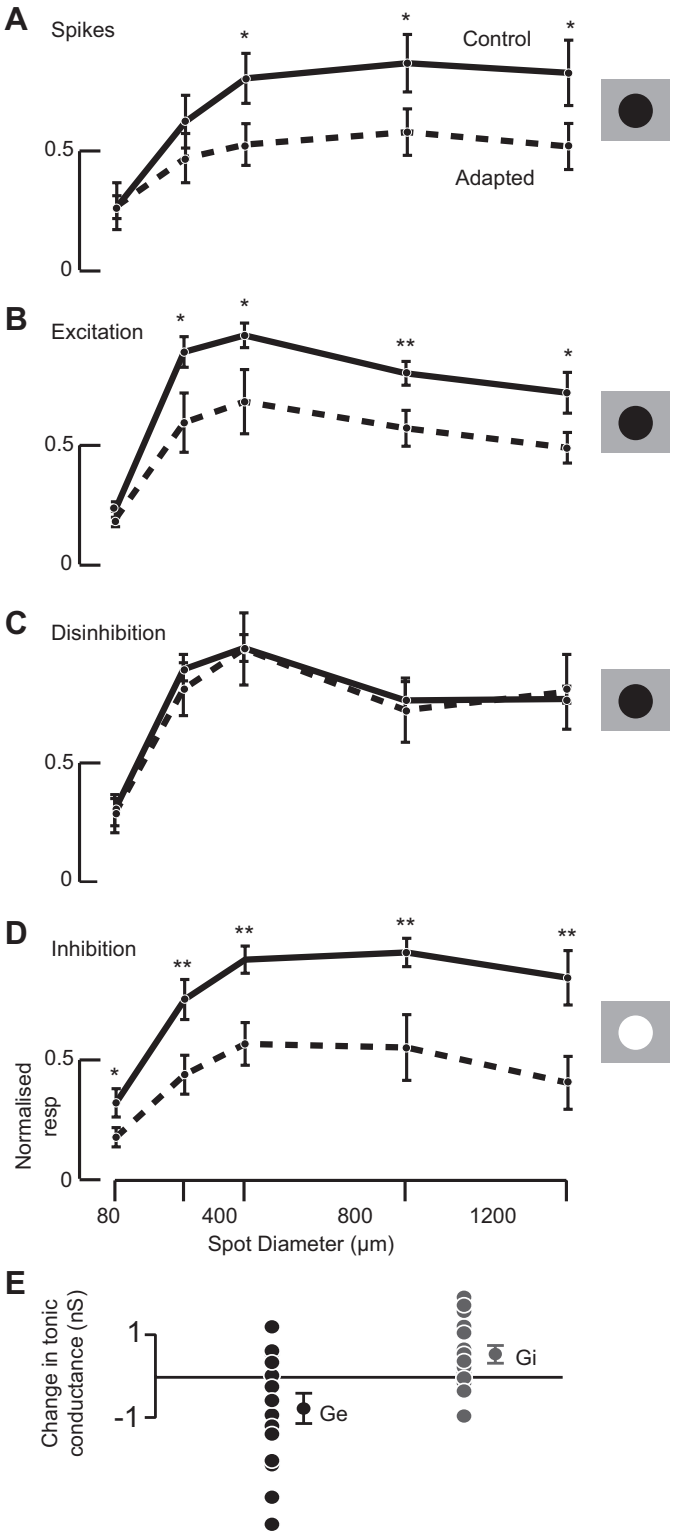

Figure 6*A* shows spatial tuning of average spike response before and during prolonged exposure to high contrast modulation. Response of each cell was normalized to the maximum obtained in the control condition and then averaged across cells. The overall impact of contrast adaptation is a reduction in response amplitude, with little effect on spatial tuning. Close inspection shows, however, that contrast adaptation did not reduce the spike response to the smallest stimulus, even though it reduced response at all other sizes, on average by 34.90% (SD 0.05, $n = 8$). Extracellular responses from an additional 11 OFF-S cells, in which we did not make whole cell recordings, showed the same pattern of response.

Figure 6*B* shows the spatial profile of excitation at light-off, before and during adaptation, averaged across 15 cells. Contrast adaptation reduces the magnitude of excitation at all stimulus sizes (by on average 30.3%, SD 6.2) and has no effect on the spatial tuning of excitation. To illustrate this we calculated SI as above: before adaptation SI was on average 0.35 (SD 0.24), and during adaptation it was 0.42 (SD 0.32; $P = 0.5$, paired Student's *t*-test). Center size and surround size were similarly unaffected by adaptation (not shown). The lack of effect on spatial tuning of excitation suggests that contrast adaptation has not changed those (inner or outer) retinal mechanisms that provide the surround of bipolar cells.

Figure 6*C* shows the impact of contrast adaptation on disinhibition at light-off. Contrast adaptation has no effect on the magnitude of disinhibition (adaptation reduced disinhibition by on average 4.0%, SD 10.3) or spatial tuning of disinhibition. Figure 6*D* shows the impact of contrast adaptation on inhibition at light-on. Inhibition is strongly reduced at all sizes (by on average 47.0%, SD 7.8), but spatial tuning is not affected. Before adaptation SI was on average 0.33 (SD 0.27), and during adaptation it was 0.44 (SD 0.34; $P = 0.3$, paired Student's *t*-test).

We further established the impact of contrast adaptation on the tonic activation of synaptic inputs to OFF-S cells (Fig. 6*E*). This measurement is independent from those obtained for light response and provides a window onto the resting state of presynaptic inputs during contrast adaptation. Contrast adaptation reduced tonic excitation by 0.73 nS (SD 1.38; $P = 0.04$) and increased tonic inhibition by 0.54 nS (SD 0.80; $P = 0.02$).

Functional implication of differential susceptibility to contrast adaptation. The observations above show that contrast adaptation has much more impact on the excitatory synaptic input at light-off than it has on the disinhibitory input. We have also shown that disinhibition is most prominent during presen-

Fig. 6. Impact of contrast adaptation on area-response function of OFF-S retinal ganglion cells. *A*: contrast adaptation reduces spike rate. Average area response for light-off during control conditions (solid line), and during adaptation to high contrast modulation of a large field (diameter 1,200 μm; dashed line). Responses were normalized to the maximum obtained in the control condition before averaging ($n = 8$ cells). *B*: contrast adaptation reduces excitatory conductance at light-off. Conventions as in *A*, except that response was averaged over 15 cells. *C*: contrast adaptation has no effect on disinhibition at light-off. Same cells and conventions as in *B*. *D*: contrast adaptation reduces inhibition at light-on. Same cells and conventions as in *B*. *E*: contrast adaptation reduces tonic excitatory conductance and increases tonic inhibitory conductance. Displaced circles represent the mean value across 15 cells. Error bars show ±SE. Significance level: $*P < 0.05$, $**P < 0.001$.

tation of a small stimulus. Together these observations lead to a strong prediction—that the impact of contrast adaptation on spike response should be less when the stimulus is very small.

Figure 7 compares the impact of adaptation on spike response and conductance, as a function of stimulus size. For this analysis we used the eight cells in which we measured contrast adaptation for conductance and spike rate. Figure 7*A* shows the ratio of disinhibition to excitation. For the smallest stimulus disinhibition is twice the amplitude of excitation, but for larger sizes disinhibition and excitation are of similar magnitude. Figure 7*B* shows the impact of contrast adaptation on excitatory and disinhibitory conductance. To characterize the impact of contrast adaptation we calculated an adaptation index (AI), AI = R(a)/R(c), where R(c) is the relevant response metric during control conditions and R(a) is that during contrast adaptation. Values larger than 1 indicate an increase in response during adaptation; values smaller than 1 indicate a reduction. Figure 7*B* shows that contrast adaptation has little impact on disinhibition at any size; AI ranged from 0.90 to 1.01 and in no case was significantly different from 1. Excitation at all sizes is reduced by contrast adaptation (AI ranging from 0.64 to 0.78). These were all significant ($P < 0.05$). Because disinhibition is more prominent at the smallest size, we expect that the impact of contrast adaptation on spike rate will be least for the smallest size. This is the case. Figure 7*C* shows the reduction in spike rate brought about by contrast adaptation: response to the smallest size is not changed by adaptation. For the smallest size AI was on average 1.02 (SD 0.08); for larger sizes it ranged from 0.59 to 0.73 (and in all cases was significant at $P < 0.05$). We conclude that contrast adaptation changes the balance of excitatory and disinhibitory inputs and that the lack of effect of contrast adaptation on disinhibition explains the lack of impact of contrast adaptation on spike response to small stimuli.

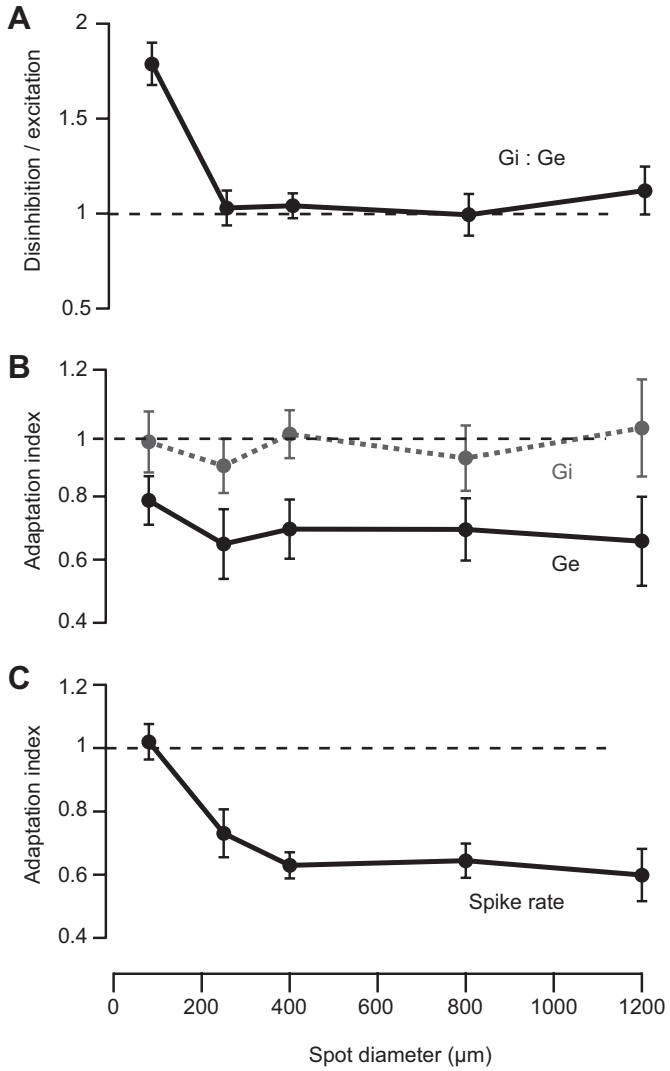

Fig. 7. Disinhibition preserves spatial acuity during contrast adaptation. *A*: relative magnitude of disinhibition (G_i) and excitation (G_e) as a function of stimulus size, obtained in the absence of contrast adaptation. Disinhibition is larger than excitation for the smallest stimulus only. *B*: impact of contrast adaptation on disinhibition (dashed line) and excitation (solid line). Adaptation index values > 1 indicate an increase in response during adaptation; values < 1 indicate a reduction. Contrast adaptation reduces excitation at all stimulus sizes but has no effect on disinhibition. *C*: impact of contrast adaptation on spike rate. Contrast adaptation reduces response to larger sizes but not the smallest size. This is consistent with the idea that disinhibition is relatively stronger at the smallest size and is unaffected by contrast adaptation.

Glycinergic and GABAergic contributions to inhibition. Previous work shows that application of strychnine, an antagonist of glycine receptors, reduces the magnitude of disinhibition at light-off and the magnitude of inhibition at light-on. Surprisingly, however, we do not know whether GABAergic mechanisms also contribute to inhibition. Here we confirmed that strychnine strongly reduces disinhibition at light-off and inhibition at light-on. In addition, we show that application of SR95531, a $GABA_A$ receptor antagonist, also reduces both forms of inhibition. In the following we pool data from tuned and untuned cells because the effect of glycine or $GABA_A$ blockade was not distinguishable.

Figure 8 shows the overall effect of strychnine (Fig. 8*A*) and SR95531 (Fig. 8*B*) on conductance in two representative cells. In each case the stimulus was a dark spot of diameter 400 μm and therefore largely confined to the receptive field center (cf. Fig. 2). The conductances shown in Fig. 8 are the sum of the tonic and stimulus-evoked components. Solid lines show stimulus-evoked conductance in control conditions (excitation in black, inhibition in gray); dashed lines show stimulus-evoked conductance during bath application of the appropriate blocker.

Figure 8*A* confirms that strychnine substantially reduces tonic inhibitory input to ganglion cells but does not quite abolish it, consistent with previous observations (Murphy and Rieke 2006; van Wyk et al. 2009). For the cell in Fig. 8*A* strychnine reduced tonic inhibitory conductance by 5.34 nS and the magnitude of stimulus-evoked disinhibition by 3.33 nS (from 4.19 nS to 0.86 nS). Strychnine also reduced stimulus-evoked excitation by 1.06 nS and at the same time increased excitatory tonic conductance by 3.92 nS. Analysis of tonic conductance across all cells tested (Fig. 8*C*) showed that application of strychnine brought about a large increase in the magnitude of tonic excitation (3.22 nS, SD 0.57, $n = 4$) and a large decrease in the magnitude of tonic inhibition (−5.40 nS, SD 0.51). In further experiments on three cells, addition of $GABA_A$ receptor antagonist SR95531 (7 μM) to the bath suppressed the remaining stimulus-evoked inhibitory conductance and further reduced tonic inhibitory conductance (data not shown).

We made similar measurements to characterize the impact of $GABA_A$ receptor blockade on each conductance, by adding

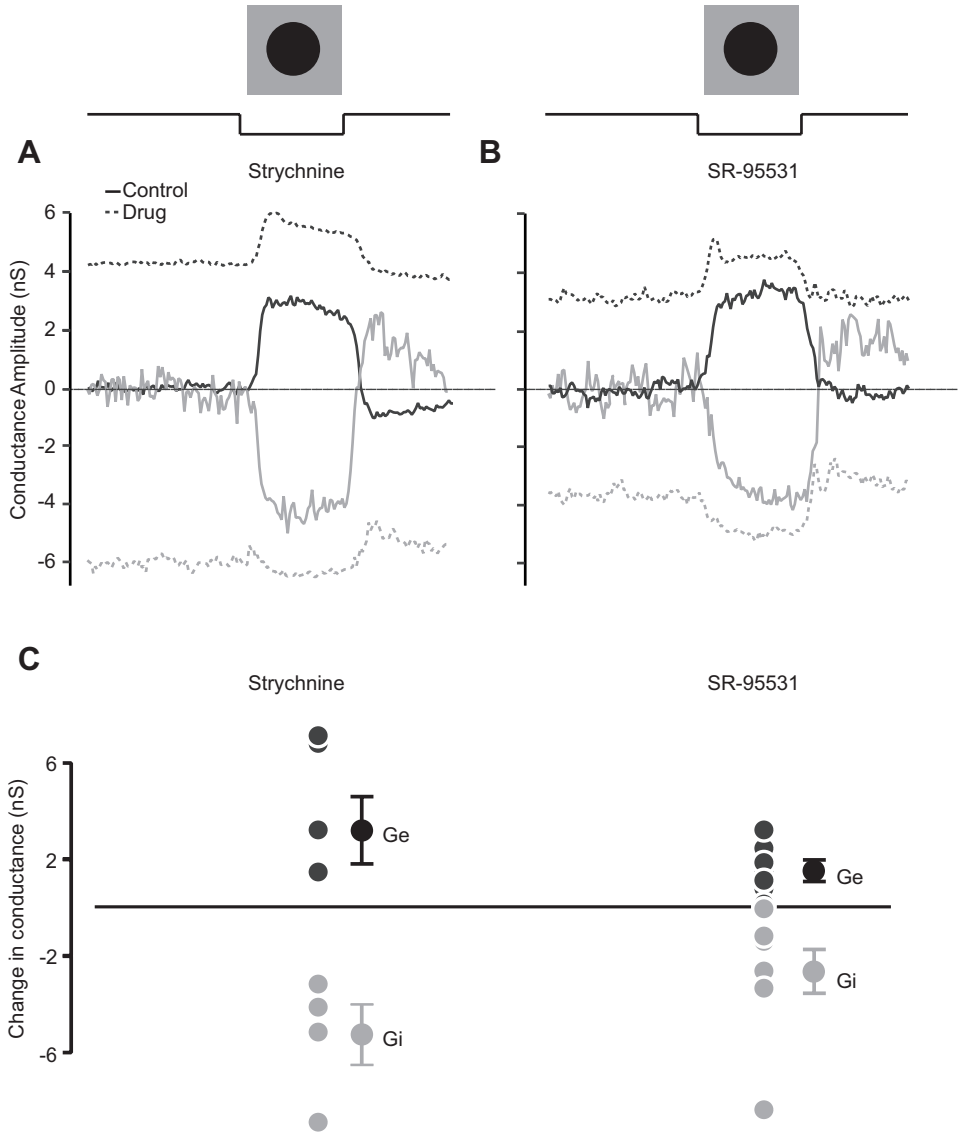

Fig. 8. Effects of strychnine and SR95531 on both stimulus-evoked and tonic conductance. *A* and *B*: solid lines show stimulus-evoked conductance in control conditions (black lines: excitation; gray lines: inhibition); dashed lines show stimulus-evoked conductance during bath application of the appropriate blocker in 2 representative cells. In each case the stimulus was a dark spot of diameter 400 μm. *A*: bath application of 2 μM strychnine increases tonic excitatory conductance and reduces stimulus-evoked excitatory conductance. Strychnine application reduces both tonic inhibitory conductance and the magnitude of stimulus-evoked disinhibition. *B*: bath application of 7 μM SR95531 increases tonic excitatory conductance and reduces stimulus-evoked excitatory conductance. SR95531 reduces both tonic inhibition and the magnitude of stimulus-evoked disinhibition. *C*: in all cells tested, tonic inhibition is reduced and tonic excitation is increased by bath application of both drugs, but the effect is stronger for strychnine. Displaced circles represent the mean across the tested cells; error bars show $\pm$1 SE.

SR95531 (7 μM) to the bath without strychnine. Figure 8*B* shows that changes in conductance during $GABA_A$ receptor blockade are similar to those observed with strychnine. For the cell in Fig. 8*B* SR95531 reduced tonic inhibitory conductance by 4.31 nS and reduced stimulus-evoked disinhibition by 2.14 nS (from 4.03 nS to 1.89 nS). SR95531 also increased tonic excitation by 3.02 nS and reduced stimulus-evoked excitatory conductance by 2.03 nS. Analysis of tonic conductance across all cells tested (Fig. 8*C*) showed that $GABA_A$ receptor blockade increased tonic excitatory conductance by 1.52 nS (SD 0.31, $n = 7$; $P < 0.001$). This was a smaller effect than that of strychnine ($P < 0.001$). Similarly, $GABA_A$ receptor blockade had a smaller effect on tonic inhibitory conductance than strychnine (decreased by 2.72 nS, SD 0.65, $P < 0.001$; vs. strychnine, $P < 0.001$). In five cells in which we tested it, further addition of 2 μM strychnine to the bath completely suppressed the remaining stimulus-evoked inhibitory conductance and further reduced tonic inhibitory conductance (data not shown).

In summary, these results show that the addition of either strychnine or SR95531 to the bathing medium reduces tonic inhibitory conductance and increases tonic excitatory conductance. The circuits that convey tonic inhibitory input to OFF-S cells therefore comprise both glycinergic and GABAergic mechanisms.

Spatial summation during blockade of inhibition. Glycinergic amacrine cells usually have narrow dendritic fields, and GABAergic amacrine cells usually have wide dendritic fields. It is therefore possible that the impact of receptor blockers on synaptic inputs to ganglion cells will depend on the size of the visual stimulus. We explored this by measuring area-response curves for the stimulus-evoked conductances before and during bath application of strychnine or SR95531.

Figure 9, *A*, *C*, and *E*, show spatial tuning of the three conductances before and during bath application of 2 μM strychnine. The stimulus-evoked conductance of each cell was normalized to the maximum obtained in the control condition and then averaged across the four cells tested. Strychnine reduced the magnitude of all stimulus-evoked synaptic inputs, both inhibitory and excitatory. As expected, strychnine had its strongest impact on the magnitude of disinhibition: 54% (SD 27) reduction for stimuli of the smallest size and from 79% to

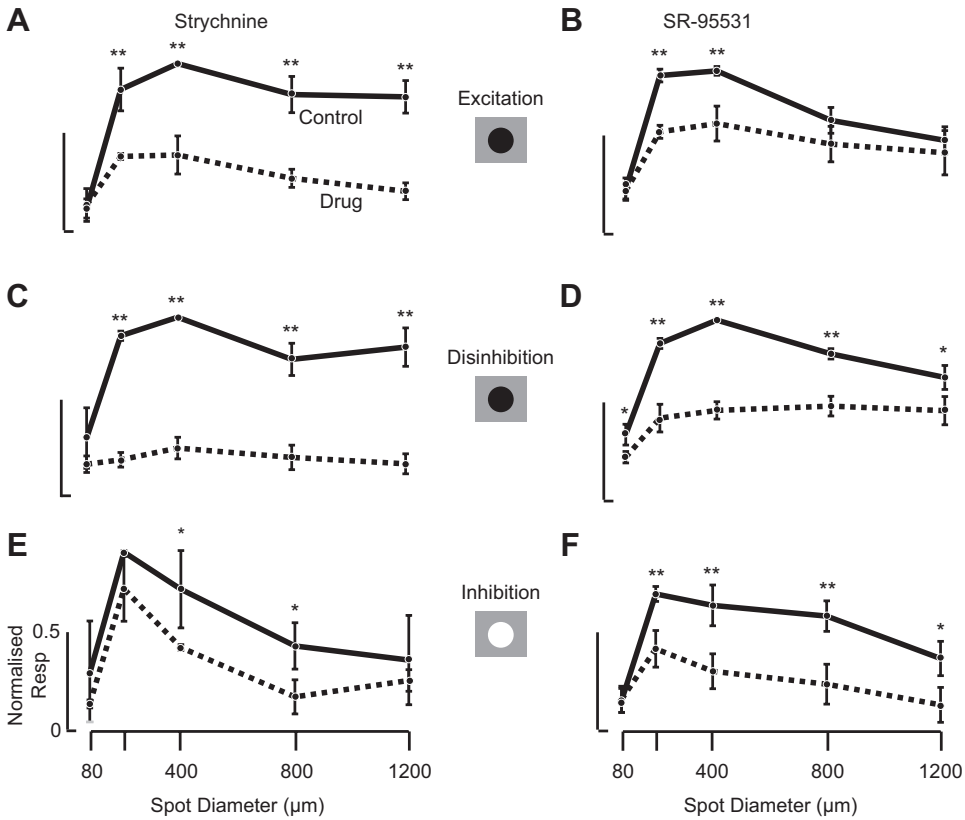

Fig. 9. Pharmacological evidence for distinct synaptic inputs onto OFF-S retinal ganglion cells. *A*, *C*, and *E*: area-response curves in control conditions and during bath application of the glycine receptor antagonist strychnine (2 μM): average of 4 cells. *B*, *D*, and *F*: area-response curves in control conditions and during bath application of the $GABA_A$ receptor antagonist SR95531 (7 μM): average of 7 cells. *A* and *B*: excitation at light-off is reduced substantially by strychnine (*A*) and less so by SR95531 (*B*). *C* and *D*: disinhibition at light-off is reduced substantially by strychnine (*C*) and less so by SR95531 (*D*). *E* and *F*: inhibition at light-on is reduced substantially by SR95531 (*F*) and less so by strychnine (*E*). Significance level: $*P < 0.05$, $**P < 0.001$. Error bars show ± 1 SE.

85% for other sizes (Fig. 9*C*). Strychnine's impact on other synaptic conductance was less marked. Excitatory inputs were reduced by 33% (SD 21) for the smallest stimulus and between 53% and 72% for other sizes (Fig. 9*A*). Inhibition at light-on was reduced by 62% (SD 42) for the smallest stimulus and between 41% and 64% for others (Fig. 9*E*).

Figure 9, *B*, *D*, and *F*, show the effect of $GABA_A$ receptor blockade on stimulus-evoked conductance (averages are based on response of 7 cells). The major effects are similar to those of strychnine, but there are some quantitative differences. First, $GABA_A$ receptor blockade has less effect on the magnitude of excitation and the magnitude of disinhibition. Excitation was reduced by 20% (SD 12) for the smallest stimulus and between 28% and 47% for the larger stimuli (Fig. 9*B*), while disinhibition was reduced by 33% (SD 18) for the smallest stimulus and between 64% and 27% for the larger stimuli (Fig. 9*D*). Second, $GABA_A$ receptor blockade has more effect on inhibition, on average reducing the response to the smallest stimulus by 24% (SD 15) and for larger sizes between 64% and 77% (Fig. 9*F*).

These observations suggest that blockade of glycine or $GABA_A$ receptors changes the magnitude of tonic and stimulus-evoked conductances. Using the DoG model, we obtained estimates of the receptive field before and during application of strychnine or SR95531. Bath application of SR95531 reduced the index of surround inhibition (SI) for the disinhibitory conductance (Fig. 9*D*), from 0.36 (SD 0.27) to 0.04 (SD 0.08; $P = 0.02$, paired *t*-test). Other analyses showed no significant effect of either drug on SI for excitation or inhibition, and no significant effect of either drug on the size of the receptive field center or surround for any of the three conductances (not shown).

DISCUSSION

Our observations show that the spatial profile of an OFF-S ganglion cell receptive field is very similar to that of its synaptic inputs. In addition, while the spatial profile of excitatory and inhibitory synaptic inputs is generally similar, there are quantitative differences. We address these issues first, and then the unexpected asymmetries in inhibitory input that are unmasked by contrast adaptation and pharmacological manipulation.

Center-surround receptive field organization in excitatory input. There is ongoing debate about the presence or absence of an inhibitory surround in the receptive field of bipolar cells. Some studies show no surround in the receptive field of bipolar cells (cat: Nelson and Kolb 1983; mouse: Berntson and Taylor 2000), but other studies find clear surrounds in various classes of bipolar cells in mouse (Pang et al. 2004), macaque monkey (Dacey et al. 2000), and goldfish (Kaneko 1973). Although our measurements were made in the same way for every cell, excitatory inputs showed clear evidence of receptive field surrounds in only 10 of 26 cells. When excitatory inputs were spatially tuned, so were inhibitory inputs and spike output. When excitatory input was not spatially tuned, neither inhibitory input nor spike output was. In other words, spatial summation as reflected in spikes is indistinguishable from that found in either excitation or disinhibition. This is important because it shows that spatial tuning in the synaptic input is both necessary and sufficient for ganglion cells to show spatial tuning in their spiking output.

In vivo measurements from lateral geniculate nucleus (LGN) of mouse show spatial tuning in the majority of cells (Grubb and Thompson 2003). We do not know the source of variability

in spatial tuning among our measurements. The variability may simply reflect functional variability in the ganglion cell population studied. An alternative possibility is that variability in strength of surround reflects differences in the physiological state of the retina that remain hidden to us. Spatial tuning of some ganglion cells in mouse does depend on luminance level (Szikra et al. 2011), and it is possible that physiological state has similar impact.

Differences in summation size for excitation and inhibition. Inhibitory inputs to OFF-sustained ganglion cells show smaller "center" size and higher sensitivity to small stimuli than excitatory inputs. Previous studies have not found any obvious variation in the receptive field size of the different classes of bipolar cells in the mouse (Berntson and Taylor 2000; Pang et al. 2004), making it unlikely that the smaller summation area of inhibition is simply due to smaller summation areas in the bipolar cell input to amacrine cells. The smaller size of inhibition is therefore surprising. If each class of amacrine cell tiles the retina, and draws convergent input from bipolar cells, then the spatial summation of inhibition should always be larger than that of excitation, because it is essentially a blurred and inverted copy of the excitatory bipolar cell input to ganglion cells. One possibility is that the smaller size of the inhibitory receptive field arises because the amacrine cells that provide the inhibition are themselves inhibited by other amacrine cells, effectively shrinking the spatial extent of their receptive field (Hsueh et al. 2008; Watanabe et al. 2000). A second possibility is that the functional input from amacrine cells is not uniform across the ganglion cell dendritic field, being relatively stronger when near the soma of the ganglion cell, and thus the center of the receptive field (Vu and Krasne 1992). Regardless, our observations show that disinhibition is particularly prominent for response to small stimuli and is therefore a determinant of spatial acuity in OFF-S ganglion cells. This is particularly the case during contrast adaptation, which may be nearer the normal viewing state (Bex et al. 2009). This observation is similar in spirit to that of Manookin et al. (2008), who show in guinea pig retina that disinhibition is relatively strong at low contrasts. Disinhibition therefore seems most important for boosting response to weak stimuli, those that are either low contrast or very small.

Blockade of $GABA_A$ receptors reduced the magnitude of the disinhibitory conductance and its spatial tuning. Assuming full blockade of $GABA_A$ receptors, and that these receptors are the major route for GABAergic input to ganglion cells (Feigenspan and Bormann 1998; Wässle et al. 1998), the remaining inhibitory conductance is provided by glycinergic amacrine cells. Lack of spatial tuning in remaining disinhibitory conductance may arise because $GABA_A$ receptors form part of the surround of glycinergic amacrine cells (Bloomfield and Xin 2000; Völgyi et al. 2002), but blockade of $GABA_A$ receptors did not reduce the spatial tuning of inhibition at light-on. We do not know whether the differences between light-off and light-on reflect variability in measurements or the action of distinct circuits.

Contrast adaptation: effects on excitation and inhibition. Contrast adaptation can be divided into two components (Baccus and Meister 2002). The fast component (10–100 ms), also called the contrast gain control, is responsible for contrast-dependent changes in the sensitivity and kinetics of ganglion cells. The slow component, which acts over seconds or minutes, is thought to regulate sensitivity but not change response kinetics. It is the slow component that we have studied here. It is well known that the magnitude of excitatory inputs to ganglion cells is reduced by prolonged exposure to high contrast (Kim and Rieke 2001; Zaghloul et al. 2005). The effect of contrast adaptation on inhibitory inputs is less clear. Early work showed that inhibitory inputs were not required for the expression of contrast adaptation in ganglion cell spike rate (Brown and Masland 2001; Manookin and Demb 2006). Beaudoin et al. (2008) showed that the kinetics of inhibitory input is also largely immune to the overall level of contrast.

Contrast adaptation does not require a change in inhibition, because excitatory inputs can themselves be reduced by contrast adaptation, as shown here and elsewhere. Furthermore, we have shown that contrast adaptation does not change the strength of the receptive field surround in the excitatory (or inhibitory) synaptic input. The inner or outer retinal inhibitory mechanisms that provide the receptive field surround of bipolar cells are therefore unlikely to be susceptible to contrast adaptation. Nevertheless, our observations show that inhibitory inputs onto OFF-S cells can be reduced by contrast adaptation. Previous work in mouse retina showed slow contrast adaptation in the mean inhibitory current onto OFF ganglion cells but did not distinguish changes in inhibitory and disinhibitory conductance (Wark et al. 2009). Both results are consistent with observations in salamander retina (Baccus and Meister 2002) that some amacrine cell classes are susceptible to contrast adaptation. Work in primate LGN is also consistent with the idea that inhibitory inputs to receptive fields are susceptible to contrast adaptation (Camp et al. 2009). Adaptation in the inhibitory input may simply reflect a reduction in the sensitivity of bipolar cells that provide input to amacrine cells, but it may reflect additional mechanisms of contrast adaptation in the amacrine cells themselves.

Our observations are consistent with contrast adaptation in both ON and OFF pathways. Measurements of excitatory conductance onto ganglion cells are, however, incapable of distinguishing modulation of ON and OFF pathway input to bipolar cells, as the same output may arise from opposite modulations of the two pathways. We cannot rule out, therefore, the possibility that contrast adaptation also modulates cross talk between ON and OFF pathways at sites distal to the ganglion cell (Werblin 2010).

Asymmetries in inhibition. In the absence of contrast adaptation, the withdrawal of inhibition at light-off and increase of inhibition at light-on appear as mirror images. During contrast adaptation, this chiral symmetry is broken: excitation at light-off and inhibition at light-on are reduced in amplitude, while disinhibition at light-off is not changed. Contrast adaptation, therefore, unmasks an unexpected asymmetry in the functional properties of inhibitory inputs. In the following we address possible explanations for this asymmetry.

One class of explanation is that both increases and decreases in inhibition reflect modulation of a single class of amacrine cells driven by ON bipolar cells but nonlinearities in this pathway cause contrast adaptation to have an asymmetric impact. It is unlikely that contrast adaptation simply changes the modulation sensitivity of ON bipolar cells or intermediate amacrine cells, because in both cases adaptation would be expected to reduce the magnitude of both disinhibition and inhibition. It is also unlikely that contrast adaptation simply

reduces the tonic activity of ON bipolar cells or intermediate amacrine cells (Baccus and Meister 2002), because in both cases adaptation would be expected to reduce the tonic inhibitory conductance; instead, tonic inhibitory input was increased by contrast adaptation (Fig. 6*E*).

More subtly, several classes of amacrine cells express voltage-gated sodium channels, the most common of which are wide-field GABAergic amacrine cells (Flores-Herr et al. 2001; Protti et al. 1997), but they also include the glycinergic AII amacrine cells (Boos et al. 1993). Contrast adaptation will bring about a sustained depolarization of the amacrine cell, reducing the fraction of available voltage-gated sodium channels (Hodgkin and Huxley 1952). Adaptation will have less effect on disinhibition at light-off than inhibition at light-on, because reductions in spike rate are not sensitive to the number of available sodium channels. Similarly, sustained depolarization during contrast adaptation may reduce the amount of postsynaptic current that can be recruited by inhibitory neurotransmitters at the synapse between amacrine and ganglion cells, by desensitizing the receptors. This desensitization would not affect capacity to signal reductions in inhibitory neurotransmitter, but it should slow down the disinhibitory response (Morke and Hartveit 2009). Our measurements were not designed to reveal the time course of response. Both these models would be consistent with increased tonic inhibitory conductance if it takes time for the presynaptic membrane to repolarize. If amacrine cells providing inhibition onto bipolar cell terminals were affected by contrast adaptation in the same way as those providing input onto ganglion cells, this might also contribute to the reduction in tonic excitation, and reduction in "disexcitation," that we observe (Fig. 6*E*).

The second class of explanation is that the currents underlying disinhibition at light-off and those underlying increases in inhibition at light-on are derived from different amacrine cells, which are differently susceptible to contrast adaptation. Glycinergic inputs from AII amacrine cells are a major contributor to both forms of inhibition (mouse: van Wyk et al. 2009; Murphy and Rieke 2006; guinea pig: Zaghloul et al. 2007). GABAergic inputs to OFF-S ganglion cells have been identified in physiological (mouse: Pang et al. 2003; Murphy and Rieke 2006) and immunohistochemical (rat: Koulen et al. 1996; primate: Grünert 2000) studies. The observations here are consistent with the idea that OFF-S retinal ganglion cells receive functional inhibition from glycinergic sources and a weaker but significant input from GABAergic sources. We note that SR95531 is a specific antagonist of $GABA_A$ receptors at concentrations near 5 μM (Hsueh et al. 2008) but can be a weak antagonist of glycine receptors at 20 μM (Wang and Slaughter 2005). We think it is unlikely that SR95531 is acting on glycine receptors in the experiments here. First, we used a concentration of 7 μM; second, application of strychnine alone or SR95531 alone reduced both tonic and stimulus-evoked inhibitory currents, but in each case some inhibitory inputs remained. When both antagonists were added to the bath, inhibitory inputs were abolished.

An attractive hypothesis is that amacrine cells providing glycinergic inhibition are not susceptible to contrast adaptation but some of those that provide GABAergic inhibition are. This may explain our observations, because $GABA_A$ receptors are relatively more important in mediating inhibition at light-on (Fig. 9) and contrast adaptation has greater impact on inhibition at light-on than disinhibition at light-off. Unless GABAergic amacrine cells in the OFF sublaminae full-wave rectify the input from OFF bipolar cells, GABAergic inhibition at light-on must be driven by ON bipolar cell inputs. These may arise if some GABAergic amacrine cells cross sublaminae of the inner plexiform layer (IPL) (some wide-field amacrine cells do: Farajian et al. 2011) but may also arise if some synapses of ON bipolar cells are displaced to the OFF sublamina of the IPL (Hoshi et al. 2009; Lauritzen et al. 2013) or via serial synaptic connections from other amacrine cells (Eggers and Lukasiewicz 2006; Roska et al. 1998; Zhang et al. 1997). Future experiments may reveal differential contributions of glycinergic and GABAergic inputs to contrast adaptation.

Reduction in stimulus-evoked excitation during removal of inhibition. It is counterintuitive that blockade of inhibitory receptors leads to a large decrease in stimulus-evoked excitation. A plausible explanation is that removal of inhibition onto bipolar cell terminals changes the resting state of the terminal and thereby reduces the capacity to signal changes in bipolar cell membrane potential. Indeed, the changes in tonic conductance that the drugs brought about were always greater than the changes in stimulus-evoked conductance. The reduction in stimulus-evoked excitation is not likely to reflect serial inhibitory processing, that is, removal of inhibition onto those amacrine cells that modulate the bipolar cell output. If that were the case we would expect a reduction in tonic excitatory conductance, but we observed increased tonic excitatory conductance.

Strychnine's effect on both tonic and stimulus-evoked conductance is consistent with its effect on OFF-sustained ganglion cells in cat retina, where strychnine increases the maintained discharge rate and reduces the stimulus-evoked spike response (Müller et al. 1988). Although we did not measure it, increased tonic excitatory conductance and decreased tonic inhibitory conductance would lead to increased maintained discharge rate. Reduction in stimulus-evoked excitatory and disinhibitory conductance should correspondingly reduce stimulus-evoked spike response.

The reduction in stimulus-evoked excitatory conductance that we see during bath application of strychnine or SR95531 has to be interpreted in conjunction with the effect of these drugs on tonic excitation: the change in tonic excitatory conductance is always larger than that of stimulus-evoked conductance. Nevertheless, we think the changes in tonic and stimulus-evoked conductance both reflect changes in the terminals of bipolar cells. Removal of inhibition onto bipolar cells will lead to depolarization of the bipolar cell synapse and consequently an increase in tonic release of glutamate. Continuous depolarization of bipolar cell terminals, however, will lead to accumulation of intracellular calcium in the synaptic terminal. This in turn inactivates calcium currents (von Gersdorff and Matthews 1996), which would cause a reduction in stimulus-evoked excitatory conductance (Herrmann et al. 2011).

We think that the drug-induced changes in excitation by the OFF pathway described here are accompanied by similar changes in the ON pathway. If this is the case, bath application of these drugs should increase the tonic release of ON bipolar cell terminals. This would in turn increase the tonic activity of ON amacrine cells, which should therefore increase the tonic inhibitory conductance onto OFF-S cells and reduce stimulus-evoked inhibitory conductance. Unfortunately, the drugs block

direct inhibitory input to the ganglion cells themselves, an effect that cannot be disambiguated from changes in presynaptic activity.

GRANTS

This work received grant support from Australian Research Council Discovery Project DP0988227. S. G. Solomon was supported by a Career Development Award from the National Health and Medical Research Council of Australia.

DISCLOSURES

No conflicts of interest, financial or otherwise, are declared by the author(s).

AUTHOR CONTRIBUTIONS

Author contributions: S.D.M., D.A.P., and S.G.S. conception and design of research; S.D.M. performed experiments; S.D.M. analyzed data; S.D.M., D.A.P., and S.G.S. interpreted results of experiments; S.D.M., D.A.P., and S.G.S. prepared figures; S.D.M., D.A.P., and S.G.S. drafted manuscript; S.D.M., D.A.P., and S.G.S. edited and revised manuscript; D.A.P. and S.G.S. approved final version of manuscript.

REFERENCES

Alonso JM, Usrey WM, Reid RC. Rules of connectivity between geniculate cells and simple cells in cat primary visual cortex. *J Neurosci* 21: 4002–4015, 2001.

Baccus SA, Meister M. Fast and slow contrast adaptation in retinal circuitry. *Neuron* 36: 909–919, 2002.

Balasubramanian V, Sterling P. Receptive fields and functional architecture in the retina. *J Physiol* 587: 2753–2767, 2009.

Beaudoin DL, Manookin MB, Demb JB. Distinct expressions of contrast gain control in parallel synaptic pathways converging on a retinal ganglion cell. *J Physiol* 586: 5487–5502, 2008.

Belgum JH, Dvorak DR, McReynolds JS. Light-evoked sustained inhibition in mudpuppy retinal ganglion cells. *Vision Res* 22: 257–260, 1982.

Berntson A, Taylor WR. Response characteristics and receptive field widths of on-bipolar cells in the mouse retina. *J Physiol* 524: 879–889, 2000.

Bex PJ, Solomon SG, Dakin SC. Contrast sensitivity in natural scenes depends on edge as well as spatial frequency structure. *J Vis* 9: 1.1–1.19, 2009.

Bloomfield SA, Xin D. Surround inhibition of mammalian AII amacrine cells is generated in the proximal retina. *J Physiol* 523: 771–783, 2000.

Boos R, Schneider H, Wässle H. Voltage- and transmitter-gated currents of AII-amacrine cells in a slice preparation of the rat retina. *J Neurosci* 13: 2874–2888, 1993.

Borg-Graham LJ. The computation of directional selectivity in the retina occurs presynaptic to the ganglion cell. *Nat Neurosci* 4: 176–183, 2001.

Boycott BB, Wässle H. The morphological types of ganglion cells of the domestic cat's retina. *J Physiol* 240: 397–419, 1974.

Brown SP, Masland RH. Spatial scale and cellular substrate of contrast adaptation by retinal ganglion cells. *Nat Neurosci* 4: 44–51, 2001.

Camp AJ, Tailby C, Solomon SG. Adaptable mechanisms that regulate the contrast response of neurons in the primate lateral geniculate nucleus. *J Neurosci* 29: 5009–5021, 2009.

Dacey D, Packer OS, Diller L, Brainard D, Peterson B, Lee B. Center surround receptive field structure of cone bipolar cells in primate retina. *Vision Res* 40: 1801–1811, 2000.

Derrington AM, Lennie P. The influence of temporal frequency and adaptation level on receptive field organization of retinal ganglion cells in cat. *J Physiol* 333: 343–366, 1982.

Eggers ED, Lukasiewicz PD. $GABA_A$, $GABA_C$ and glycine receptor-mediated inhibition differentially affects light-evoked signaling from mouse retinal rod bipolar cells. *J Physiol* 572: 215–225, 2006.

Enroth-Cugell C, Robson JG. The contrast sensitivity of retinal ganglion cells of the cat. *J Physiol* 187: 517–552, 1966.

Farajian R, Pan F, Akopian A, Völgyi B, Bloomfield SA. Masked excitatory crosstalk between the ON and OFF visual pathways in the mammalian retina. *J Physiol* 589: 4473–4489, 2011.

Feigenspan A, Bormann J. GABA-gated Cl^- channels in the rat retina. *Prog Retin Eye Res* 17: 99–126, 1998.

Flores-Herr N, Protti DA, Wässle H. Synaptic currents generating the inhibitory surround of ganglion cells in the mammalian retina. *J Neurosci* 21: 4852–4863, 2001.

von Gersdorff H, Matthews G. Calcium-dependent inactivation of the calcium current in synaptic terminals of retinal bipolar neurons. *J Neurosci* 15: 115–122, 1996.

Grubb MS, Thompson ID. Quantitative characterization of visual response properties in the mouse dorsal lateral geniculate nucleus. *J Neurophysiol* 90: 3594–3607, 2003.

Grünert U. Distribution of GABA and glycine receptors on bipolar and ganglion cells in the mammalian retina. *Microsc Res Tech* 50: 130–140, 2000.

Herrmann R, Heflin SJ, Hammond T, Lee B, Wang J, Gainetdinov RR, Caron MG, Eggers ED, Frishman LJ, McCall MA, Arshavsky VY. Rod vision is controlled by dopamine-dependent sensitization of rod bipolar cells by GABA. *Neuron* 72: 101–110, 2011.

Hodgkin AL, Huxley AF. A quantitative description of membrane current and its application to conduction and excitation in nerve. *J Physiol* 117: 500–544, 1952.

Hoshi H, Liu WL, Massey SC, Mills SL. ON inputs to the OFF layer: bipolar cells that break the stratification rules of the retina. *J Neurosci* 29: 8875–8883, 2009.

Hsueh HA, Molnar A, Werblin FS. Amacrine-to-amacrine cell inhibition in the rabbit retina. *J Neurophysiol* 100: 2077–2088, 2008.

Kaneko A. Receptive field organization of bipolar and amacrine cells in the goldfish retina. *J Physiol* 235: 133–153, 1973.

Kim KJ, Rieke F. Temporal contrast adaptation in the input and output signals of salamander retinal ganglion cells. *J Neurosci* 21: 287–299, 2001.

Kim KJ, Rieke F. Slow Na^+ inactivation and variance adaptation in salamander retinal ganglion cells. *J Neurosci* 23: 1506–1516, 2003.

Koulen P, Malitschek B, Kuhn R, Wässle H, Brandstatter JH. Group II and group III metabotropic glutamate receptors in the rat retina: distributions and developmental expression patterns. *Eur J Neurosci* 8: 2177–2187, 1996.

Lauritzen JS, Anderson JR, Jones BW, Watt CB, Mohammed S, Hoang JV, Marc RE. ON cone bipolar cell axonal synapses in the OFF inner plexiform layer of the rabbit retina. *J Comp Neurol* 521: 977–1000, 2013.

Manookin MB, Beaudoin DL, Ernst ZR, Flagel LJ, Demb JB. Disinhibition combines with excitation to extend the operating range of the OFF visual pathway in daylight. *J Neurosci* 28: 4136–4150, 2008.

Manookin MB, Demb JB. Presynaptic mechanism for slow contrast adaptation in mammalian retinal ganglion cells. *Neuron* 50: 453–464, 2006.

Di Marco S, Nguyen VA, Bisti S, Protti DA. Permanent functional reorganization of retinal circuits induced by early long-term visual deprivation. *J Neurosci* 29: 13691–13701, 2009.

Molnar A, Werblin F. Inhibitory feedback shapes bipolar cell responses in the rabbit retina. *J Neurophysiol* 98: 3423–3435, 2007.

Morke SH, Hartveit E. Properties of glycine receptors underlying synaptic currents in presynaptic axon terminals of rod bipolar cells in the rat retina. *J Physiol* 587: 3813–3830, 2009.

Müller F, Wässle H, Voigt T. Pharmacological modulation of the rod pathway in the cat retina. *J Neurophysiol* 59: 1657–1672, 1988.

Murphy GJ, Rieke F. Network variability limits stimulus-evoked spike timing precision in retinal ganglion cells. *Neuron* 52: 511–524, 2006.

Nelson R, Kolb H. Synaptic patterns and response properties of bipolar and ganglion cells in the cat retina. *Vision Res* 23: 1183–1195, 1983.

Pang J, Gao F, Wu SM. Light-evoked excitatory and inhibitory synaptic inputs to ON and OFF α ganglion cells in the mouse retina. *J Neurosci* 23: 6063–6073, 2003.

Pang JJ, Gao F, Wu SM. Light-evoked current responses in rod bipolar cells, cone depolarizing bipolar cells and AII amacrine cells in dark-adapted mouse retina. *J Physiol* 558: 897–912, 2004.

Platkiewicz J, Brette R. Impact of fast sodium channel inactivation on spike threshold dynamics and synaptic integration. *PLoS Comput Biol* 7: e1001129, 2011.

Protti DA, Gerschenfeld HM, Llano I. GABAergic and glycinergic IPSCs in ganglion cells of rat retinal slices. *J Neurosci* 17: 6075–6085, 1997.

Rodieck RW. Quantitative analysis of cat retinal ganglion cell response to visual stimuli. *Vision Res* 5: 583–601, 1965.

Rodieck RW, Stone J. Analysis of receptive fields of cat retinal ganglion cells. *J Neurophysiol* 28: 832–849, 1965.

Roska B, Nemeth E, Werblin FS. Response to change is facilitated by a three-neuron disinhibitory pathway in the tiger salamander retina. *J Neurosci* 18: 3451–3459, 1998.

Sun W, Li N, He S. Large-scale morphological survey of mouse retinal ganglion cells. *J Comp Neurol* 451: 115–126, 2002.

Szél A, Röhlich P, Caffé AR, Juliusson B, Aguirre G, Van Veen T. Unique topographic separation of two spectral classes of cones in the mouse retina. *J Comp Neurol* 325: 327–342, 1992.

Szikra T, Farrow K, Roska B. Cone-mediated circuit switch activates lateral inhibition in a retinal ganglion cell (Abstract). In: *ARVO Meet Abstr* 52: 4569, 2011.

Taylor WR, Vaney DI. Diverse synaptic mechanisms generate direction selectivity in the rabbit retina. *J Neurosci* 22: 7712–7720, 2002.

Völgyi B, Xin D, Bloomfield SA. Feedback inhibition in the inner plexiform layer underlies the surround-mediated responses of AII amacrine cells in the mammalian retina. *J Physiol* 539: 603–614, 2002.

Vu E, Krasne F. Evidence for a computational distinction between proximal and distal neuronal inhibition. *Science* 255: 1710–1712, 1992.

Wang P, Slaughter MM. Effects of GABA receptor antagonists on retinal glycine receptors and on homomeric glycine receptor α-subunits. *J Neurophysiol* 93: 3120–3126, 2005.

Wang YV, Weick M, Demb JB. Spectral and temporal sensitivity of cone-mediated responses in mouse retinal ganglion cells. *J Neurosci* 31: 7670–7681, 2011.

Wark B, Fairhall A, Rieke F. Timescales of inference in visual adaptation. *Neuron* 61: 750–761, 2009.

Wässle H. Parallel processing in the mammalian retina. *Nat Rev Neurosci* 5: 747–757, 2004.

Wässle H, Koulen P, Brandstätter JH, Fletcher EL, Becker CM. Glycine and GABA receptors in the mammalian retina. *Vision Res* 38: 1411–1430, 1998.

Watanabe SI, Koizumi A, Matsunaga S, Stocker JW, Kaneko A. GABA-mediated inhibition between amacrine cells in the goldfish retina. *J Neurophysiol* 84: 1826–1834, 2000.

Wei W, Elstrott J, Feller MB. Two-photon targeted recording of GFP-expressing neurons for light responses and live-cell imaging in the mouse retina. *Nat Protoc* 5: 1347–1352, 2010.

Weick M, Demb JB. Delayed-rectifier K channels contribute to contrast adaptation in mammalian retinal ganglion cells. *Neuron* 71: 166–179, 2011.

Werblin FS. Six different roles for crossover inhibition in the retina: correcting the nonlinearities of synaptic transmission. *Vis Neurosci* 27: 1–8, 2010.

van Wyk M, Taylor WR, Vaney DI. Local edge detectors: a substrate for fine spatial vision at low temporal frequencies in rabbit retina. *J Neurosci* 26: 13250–13263, 2006.

van Wyk M, Wässle H, Taylor WR, Wassle H. Receptive field properties of ON- and OFF-ganglion cells in the mouse retina. *Vis Neurosci* 26: 297–308, 2009.

Zaghloul KA, Boahen K, Demb JB. Different circuits for ON and OFF retinal ganglion cells cause different contrast sensitivities. *J Neurosci* 23: 2645–2654, 2003.

Zaghloul KA, Boahen K, Demb JB. Contrast adaptation in subthreshold and spiking responses of mammalian Y-type retinal ganglion cells. *J Neurosci* 25: 860–868, 2005.

Zaghloul KA, Manookin MB, Borghuis BG, Boahen K, Demb JB. Functional circuitry for peripheral suppression in mammalian Y-type retinal ganglion cells. *J Neurophysiol* 97: 4327–4340, 2007.

Zhang J, Jung CS, Slaughter MM. Serial inhibitory synapses in retina. *Vis Neurosci* 14: 553–563, 1997.